JOURNAL OF GEOPHYSICAL RESEARCH, VOL. 114, F02007, doi:10.1029/2008JF000999, 2009

Simulating and understanding sand wave variation: A case study of the Golden Gate sand waves

F. Sterlini,[1] S. J. M. H. Hulscher,[1] and D. M. Hanes[2]

Received 19 February 2008; revised 11 December 2008; accepted 10 February 2009; published 21 April 2009.

[1] In this paper we present a detailed comparison between measured features of the Golden Gate sand wave field and the results of a nonlinear sand wave model. Because the Golden Gate sand waves exhibit large variation in their characteristics and in their environmental physics, this area gives us the opportunity to study sand wave variation between locations, within one well-measured, large area. The nonlinear model used in this paper is presently the only tool that provides information on the nonlinear evolution of large-amplitude sand waves. The model is used to increase our understanding of the coupling between the variability in environmental conditions and the sand wave characteristics. Results show that the model is able to describe the variation in the Golden Gate sand waves well when both the local oscillating tidal current and the residual current are taken into account. Current and water depth seem to be the most important factors influencing sand wave characteristics. The simulation results give further confidence in the underlying model hypothesis and assumptions.

Citation: Sterlini, F., S. J. M. H. Hulscher, and D. M. Hanes (2009), Simulating and understanding sand wave variation: A case study of the Golden Gate sand waves, *J. Geophys. Res.*, *114*, F02007, doi:10.1029/2008JF000999.

1. Introduction

[2] Several patches of rhythmic bed forms are clearly visible on the sea bed near the Golden Gate entrance of San Francisco Bay (Figure 1). Bed forms are typical features in shallow seas, though their shape and morphology are highly variable. We classify the bed forms seen in Figure 1 as sand waves in accordance with their geometrical scale and the dominant tidal flows in the region. In this area, sand wave lengths are around 100 m, sand wave heights are typically about 5 m, and they migrate several meters per year. Because of their scale and migration, sand waves are expected to influence the tidal currents and play an important role in the sediment dynamics in the region. Understanding the sediment flux in the vicinity of the Golden Gate inlet is integral to the proper management of sediment in the entire Bay region. The Golden Gate sand wave field has been measured with high resolution over the past few years. The measurements show dynamic sand waves with large variation in shape and orientation. The water depth (15–70 m) and peak tidal flow velocity (0.3–1.5 m/s) also exhibit large spatial variations. However, it is yet unclear which environmental factors contribute most to the observed sand wave variations.

[3] Numerical models based on stability analyses have been used to understand the formation and evolution of sand waves [*Hulscher and Van den Brink*, 2001; *Besio et al.*, 2003a, 2004; *Van der Veen et al.*, 2006]. Most modeling research has been carried out in the linear regime, i.e., both the interaction between the flow and the sea bed, and the sand wave growth is assumed to be linear. The assumption of linearity only holds for the initial stage of sand wave growth. Linear modeling therefore excludes information on the final shape of the sand waves because there nonlinear interactions become important, leading to a decrease in sand wave growth, a change of the sand wave form and in the end a final sand wave shape that is in equilibrium with the flow. In the few nonlinear model studies to date, the influence of environmental processes has not been studied in detail [*Németh et al.*, 2006, 2007; *Van den Berg and Van Damme*, 2006]. Model results are sometimes compared with data from single transects to test the accuracy of model results and the underlying physical hypotheses [*Van den Berg and Van Damme*, 2006; *Németh et al.*, 2007]. A comparison between observations and the model results to test in detail the models ability to describe all sand wave characteristics and its ability to deal with variation between locations has not yet been accomplished.

[4] We are interested in the physical causes of variation in sand wave characteristics between different locations. We aim to better understand the physical background of the morphological features. Our main question in this paper is: "Can we explain sand wave variation between locations with differing physical environmental processes using a simplified nonlinear model?". To answer this question we compare the Golden Gate sand wave observations with the results of the nonlinear sand wave model. As the Golden

[1] Water Engineering and Management, Faculty of Engineering Technology, University of Twente, Enschede, Netherlands.
[2] Coastal and Marine Geology Program, U.S. Geological Survey, Santa Cruz, California, USA.

0148-0227/09/2008JF000999$09.00

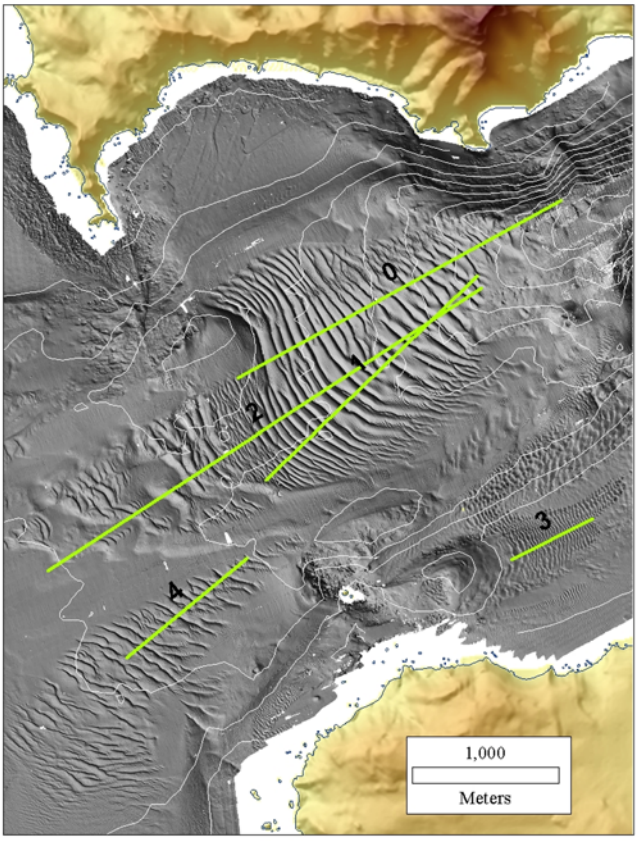

Figure 1. Mouth of San Francisco Bay entrance with the described sand wave transects.

Gate sand waves show large variation in their characteristics and in their physical environment, this area gives us the opportunity to study sand wave variation within a single, well measured, large area. The model used in this paper is presently the only tool that gives information on nonlinear large amplitude sand wave evolution. The model is used to increase our understanding of the coupling between environmental variation and sand wave characteristics. Because the underlying theory (section 3) and the model simplifications have not been tested previously in detail against data, our second aim is to further test the underlying theory. If the model is able to predict sand wave variation reasonably, then it could also be used to predict sand wave characteristics in other locations, perhaps even where no measurements are available. As the main strength of the nonlinear model is the inclusion of the sand wave height and shape, our focus is on the sand wave morphology and less on the dynamics (time evolution and migration). Another reason we do not focus on the dynamics here, is that the migration patterns of the Golden Gate sand waves are complicated and recent measurements are still being analyzed and interpreted (section 2).

[5] We start with describing the mouth of San Francisco Bay and the measured sand wave characteristics in more detail in section 2. The numerical model is described in section 3. The model results are compared with the field data and a sensitivity analysis is carried out for important model parameters (section 4). Discussion and conclusions follow in sections 5 and 6.

2. Measurements

2.1. General

[6] San Francisco Bay is located on the west coast of the USA and is connected to the Pacific Ocean through the Golden Gate (Figure 1). Maximum tidal currents through the channel typically exceed 2.5 m/s, and the channel has scoured down to bedrock with a maximum depth of 113 m.

[7] Sand waves exist on both sides of the Golden Gate Channel. The 4 km^2 sand wave field outside the Golden Gate Channel (Figure 1) has recently been investigated by *Barnard et al.* [2006]. The entire sand wave field in the mouth of San Francisco Bay was mapped in 2004, 2005, 2007. The region along the centerline of the sand waves (transect 0 in Figure 1) was mapped four times in 2004: on 17, 18, 25, and 30 October; three times in 2005: on 17, 18 September and 30 October; and on 4 February 2007. The repeated surveys focused on 19 distinct contiguous bed forms in water depths between approximately 35 and 80 m, shallowing seaward of the Golden Gate approaching the large ebb tidal shoal. Sand wave shapes range from ebb dominated to symmetric. Wavelengths are between 32 and 145 m, and the mean sand wave height is 4.1 m. Grain size on the bed surface of these sand waves is coarse (typically 0.8 mm).

[8] Over the entire area, the sand waves have diverse shapes and sizes. The largest sand wave has a wavelength of 220 m and a height of 10 m. Net migration varies over time, and was approximately 5–10 m/a seaward in the 2004–2005 time frame. Crest positions can oscillate approximately 3 m/d depending on the daily tidal current patterns [*Barnard et al.*, 2006].

[9] *Cheng and Gartner* [1984] measured flow velocities near the mouth of San Francisco Bay ranging between 0.3 and 1.3 m/s. Recent measurements show that velocities in the Golden Gate channel often exceed the 2.5 m/s [*Barnard et al.*, 2006]. A hydrodynamic 2-D horizontal simulation shows tidal flows of comparable magnitudes [*Barnard et al.*, 2007].

[10] Because of this large range in both the sand wave shape and the physical environment, the Golden Gate sand waves present an excellent opportunity to investigate the relation between the environmental conditions and the sand wave characteristics.

2.2. Transects

[11] To study sand wave variation, 4 transects (Figure 1, transects 1–4) are used for comparison with the numerical results described in section 4. Table 1 lists measurement characteristics and typical flow velocities for each transect. Table 2 shows the sand wave characteristics, defined using the Bedform Tracking Tool (BTT) of *Van der Mark et al.* [2007]. The four transects are chosen such that they represent the range of physical conditions and sand wave characteristics in the entire sand wave field. Transects are taken approximately perpendicular to the sand wave crests.

[12] Transects 1 and 2 run through some of the biggest sand waves in the middle of the field. The transects are 2

Table 1. Information About the Field Characteristics and Measurement Characteristics on the Transects[a]

Transect	Length (m)	Water Depth (m)	Number of Points	Interval (m)	U_{osc}'84 (m/s)	U_{osc} D3D (m/s)	U_{uni} D3D (m/s)
1	2002	40–70	200 + 1	10	0.4–1.2	1.3	0.5
2	3520	30–70	176 + 1	20	0.4–1.2	1.1	0.5
3	620	13–18	124 + 1	5	0.45	0.5	−0.3
4	1065	32–40	213 + 1	5	0.6–1.2	1.1	0.3

[a]Number of points are the number of data points over the transects. U_{osc} is the oscillating part of the current, estimated from both *Cheng and Gartner* [1984] (U_{osc}'84) and Delft3D simulations (U_{osc} D3D). The unidirectional flow component is also estimated using the Delft3D output (U_{uni} D3D).

and 3.5 km long, respectively, and each transect contains approximately 30 sand waves. For transect 1, the largest sand waves (lengths up to 110 m) are found in the deeper, steeper sloping area (Figure 2). Sand wave height ranges up to 7 m in this area and is on average 4.6 m. Transect 2 (Figure 2) has two large sand waves in the shallower part (seaward edge), with wave lengths around 300 m. These two seem to stand apart from the other sand waves on the transect, where wave lengths are closer to 100 m. The waves on transect 2 are on average 3.4 m high and, like on transect 1, asymmetric and directed toward the Pacific. Measurements [*Cheng and Gartner*, 1984] and a hydrodynamic 2DH simulation of the tidal flow [*Barnard et al.*, 2007] show that the flow velocities are high in this part of the sand wave field, with maxima between 1.0 and 1.5 m/s, and averaged over a tide, directed toward the southwest, approximately perpendicular to the sand wave crests. Transect 3 (Figure 2) is located at the shallow southern part of the mouth; it has around 25 sand waves over a length of 620 m. The flow velocity is lower than in the center of the mouth (maximum around 0.5 m/s), and averaged over the tide, directed toward the Golden Gate. The water depth is relatively shallow and the sand waves are small compared to the first two transects. Sand wave heights are less than 1 m and wavelengths are around 25 m. Within the transect the variation is small. Transect 4 is situated just outside the San Francisco Bay mouth. Here the sand waves are slightly smaller than on the first two transects (mean height 2.3 m and mean length 80 m), and the shape is again asymmetric, oriented toward the southwest. Over the transect, sand waves are more uniform in the middle and become more irregular toward both the deeper and the shallower edge. The transect covers around 15 sand waves.

[13] Sand wave migration has been estimated for transect 0, using repeated surveys. Figure 3 shows a section of transect 0 measured four times over a 4 year period. Between October 2004–2005 these sand waves migrated seaward, but between October 2005 and February 2007 they appear to have migrated landward, in spite of their seaward directed shape asymmetry measured during each survey! Then between February 2007 and April 2008 they migrated seaward again. The migration of the sand waves is obviously variable in time, and initial investigations of the entire sand wave field indicate that migration varies in space as well. This is currently a topic of active investigation, but at this time the migration of the sand waves is not well understood.

3. Sand Wave Code

[14] The Sand Wave Code (hereafter denoted by SWC) used in this study is based on an idealized model by *Németh et al.* [2006] that was further developed by *Van den Berg and Van Damme* [2006]. It is a two dimensional vertical model, which was developed specifically to describe sand wave evolution from its generation to its fully grown state. For sand wave fields in the Southern part of the North Sea the SWC has shown good results in describing the wavelength, height and migration [*Németh et al.*, 2002, 2007]. However, an in depth comparison with field data has not yet been accomplished.

[15] Results of the idealized model are intended to represent general trends in the data. The goal of the SWC is to reproduce the general sand wave patterns; because of nonlinear and stochastic behavior of sediment in turbulent flow, we do not attempt to reproduce the details within sand wave transects.

[16] For the range of conditions studied in this work, the final sand wave height for any particular forcing condition exhibits some uncertainty (about 15%), due to possible fluctuations in the final shape. The SWC accuracy in sand wave length is determined by the length intervals utilized, which in this study ranges from 20 to 30 meters.

3.1. Sand Wave Theory

[17] Sand waves are formed because of interaction between a sandy seabed and a tidal flow. Sand waves occur as free instabilities in this system, i.e., there is no direct

Table 2. Sand Wave Characteristics From the Bedform Tracking Tool for the Transects[a]

	H_{sw} (m)			L_{sw} (m)			Landward Side Slope			Seaward Side Slope		
Profile	Minimum	Mean	Maximum	Minimum	Mean	Maximum	Minimum	Mean	Maximum	Minimum	Mean	Maximum
0	0.9	4.1	6.5	32	85	144	0.03	0.10	0.30	0.05	0.16	0.27
1	2.5	4.7	6.9	70	88	110	0.05	0.14	0.23	0.07	0.14	0.24
2	0.7	3.4	7.5	60	129	300	0.01	0.09	0.18	0.01	0.07	0.19
3	0.1	0.5	0.7	15	24	50	0.02	0.09	0.14	0.01	0.04	0.06
4	1.7	2.4	3.3	65	79	85	0.03	0.05	0.06	0.10	0.14	0.18

[a]H_{sw} is the sand wave height, and L_{sw} is the sand wave length. Landward and seaward for the slopes refers to the transect figures (Figures 1 and 2).

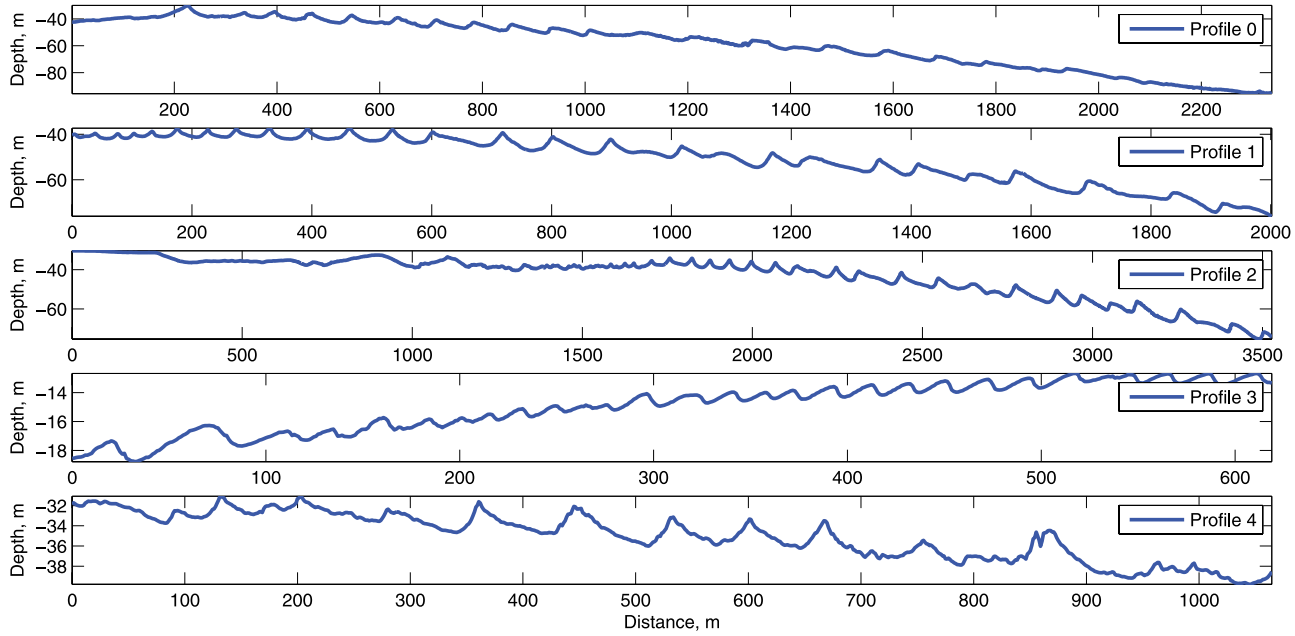

Figure 2. Transect 0–4. The left side is the seaward side of the transects. Note that the scales vary per transect.

relation between the scales related to the forcing (tide) and those related to the morphological feature (sand wave) [*Dodd et al.*, 2003]. Sand wave occurrence can be understood only if the feedback mechanism between the forcing and the seabed is taken into account. *Hulscher* [1996] described this mechanism of self organization for sand waves, as summarized below.

[18] Starting from a flat bed with an oscillating current, small perturbations of the sea floor cause small perturbations in the flow field and vice versa. The bed can be either stable, which means that all bed perturbations will be damped, or unstable, which means that certain bed perturbations will grow and the sea bed is changed. This growth is a result of higher flow velocity where the water depth decreases in the downstream direction. This causes a slightly higher flow velocity on the uphill relative to downhill sides at the perturbation (Figure 4). Because of

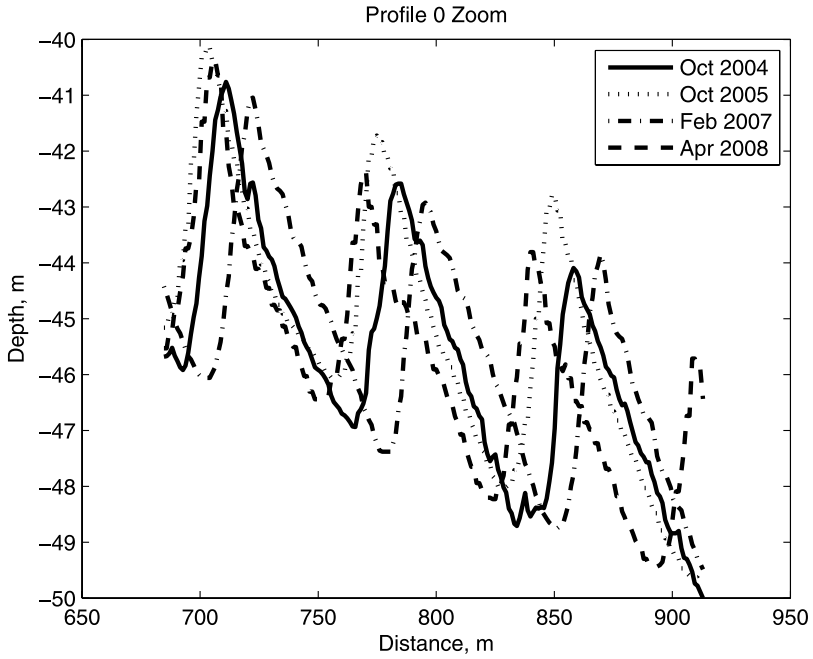

Figure 3. Repeated surveys on transect 0 show the sand wave migration in time. Both the migration rate and the migration direction changes in time.

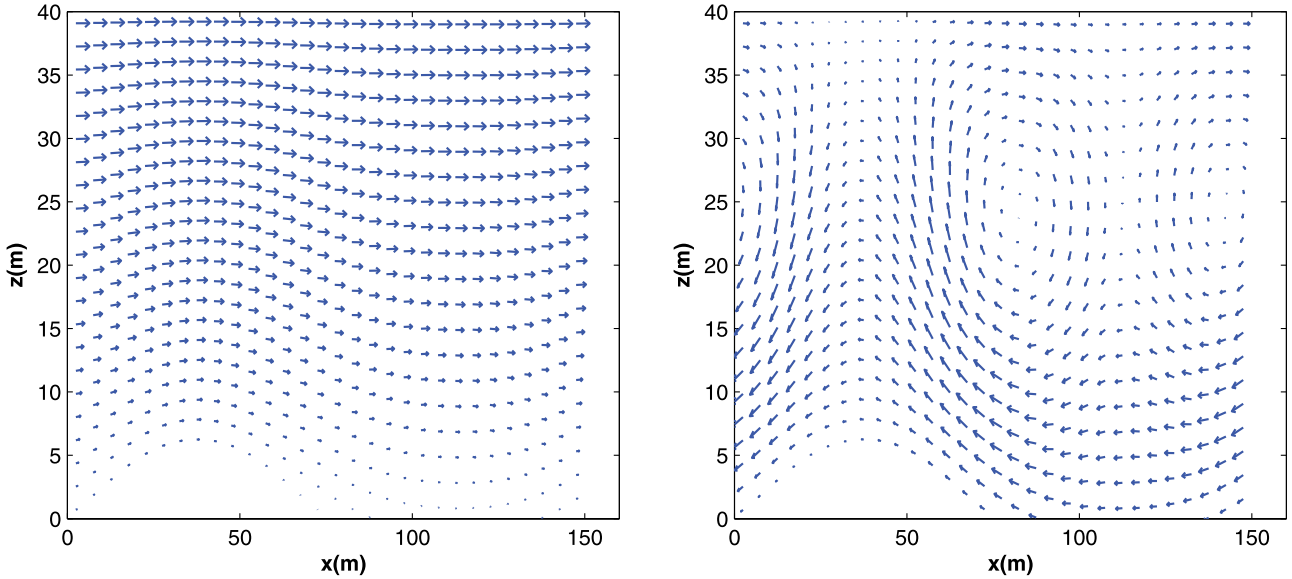

Figure 4. Flow patterns over a sand wave at two moments during the tidal cycle. (left) The flow at its peak (arrows represents flow magnitude multiplied by 2), and (right) the flow at reversal (arrows represents flow magnitude multiplied by 8).

the oscillating character of the flow this happens alternately on both sides of the perturbation, causing it to grow rather than migrate.

[19] If the flow field is changed such that, averaged over the tidal cycle, small vertical residual circulation cells occur (Figure 5), then these cells cause small net sediment transport toward the crest of a perturbation, thereby causing growth. Depending on the circumstances such as flow velocity and water depth, perturbations with different lengths will show different growth/decay rates. We refer to the perturbation which causes the fastest initial growth as the fastest growing mode.

[20] For small amplitude sand waves, growth can be described as linear, because the nonlinear feedback mechanisms between the flow and the bed form are still negligible. However, as sand waves grow larger, nonlinear effects become important. There are several indicators supporting the assumption that sand waves are only weakly nonlinear: their amplitude is generally smaller than 20% of the water depth and the predicted fastest growing wave length (growth in height) is close to the observed wave length. Assuming only weak nonlinearity, the dominating wavelength for linear bed forms will be close to the one dominating in the nonlinear regime, i.e., for full grown sand waves. Subsequently, the fastest growing mode indicates the sand wave length that should be close to the dominant equilibrium wave length in reality for weakly nonlinear systems [*Dodd et al.*, 2003].

3.2. Physical and Numerical Background

[21] As the SWC is idealized, it uses simple input and boundary conditions, to study morphological features at the morphodynamic timescale, i.e., decades. Specific physical processes and conditions are only included in the model when they are important for sand wave evolution.

[22] We start simulations by prescribing sinusoidal, small amplitude, bed waves. Using the bathymetry, a tidal flow is calculated over the domain. As the flow changes over a timescale of hours and the morphology over much longer timescales, the bathymetry is assumed to be invariant within a single tidal cycle ($h(x)$ instead of $h(x, t)$). Once the tidal flow is known, the bed changes are calculated over this typical tidal flow pattern, using a sediment transport equation. This is repeated until the bed evolution exceeds a certain value, after which a new flow pattern is calculated. This, in turn, affects the bed evolution and so the process is iterative. In this way, we are able to simulate the morphological timescale accurately, while reducing computation

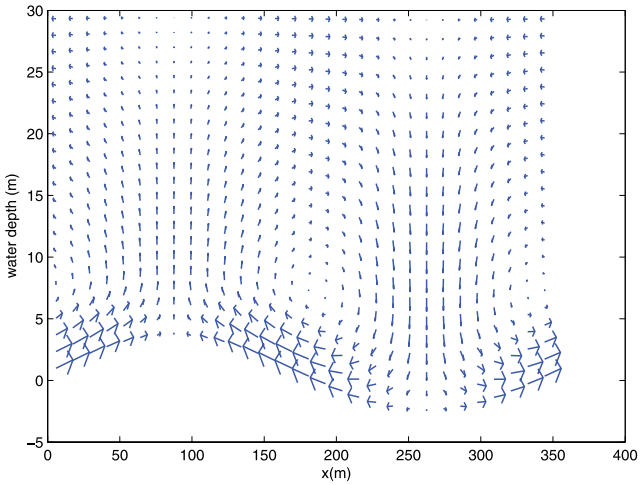

Figure 5. Residual circulation, averaged over one tidal cycle. In this case the interaction between the flow and the bed perturbation will lead to growth of the perturbation.

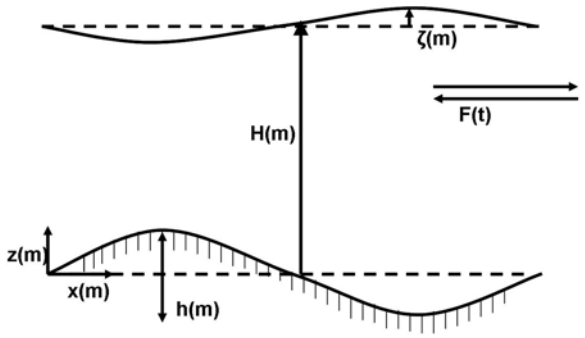

Figure 6. Sketch of the domain set up in the model.

times, as the flow calculations are the most time-consuming part.

[23] The SWC consists of the hydrostatic flow equations for 2DV incompressible flow (equations (1) and (2))

$$\frac{\partial u}{\partial x}+\frac{\partial w}{\partial z}=0 \tag{1}$$

$$\frac{\partial u}{\partial t}+u\frac{\partial u}{\partial x}+w\frac{\partial w}{\partial z}=-g\frac{\partial \zeta}{\partial x}+A_v\frac{\partial^2 u}{\partial z^2}+F(t). \tag{2}$$

In these equations x and z represent the horizontal and vertical directions and u and w the horizontal and vertical flow velocities. The variable t denotes time, ζ is the water surface elevation, g is the constant of gravity and A_v is the constant eddy viscosity. See Figure 6 for a sketch of the model geometry. The tidal flow is prescribed as a sinusoidal current by means of a forcing F (equation (3)). Variation due to spring neap tide or seasonal changes is not included. This is consistent with other studies on sand waves [*Van den Berg and Van Damme*, 2006; *Németh et al.*, 2002; *Besio et al.*, 2003b]

$$F(t)=F_0+F_s\sin(\omega t)+\mathrm{F}_c\cos(\omega t). \tag{3}$$

Here ω is the angular frequency, $1.4\times10^{-4}\ \mathrm{s}^{-1}$, and F_0, F_s, and F_c are constants depending on the tidal velocity. Boundary conditions at the bed prohibit flow perpendicular to the bottom (equation (4)). Further, a partial slip condition compensates for the constant eddy viscosity, which overestimates the eddy viscosity near the bed (equation (5)). The parameter S denotes the amount of slip, with $S = 0$ indicating perfect slip and $S = \infty$ indicating no slip. At the water surface, there is no friction at and no flow through the surface (equations (6) and (7))

$$w-u\frac{\partial h}{\partial x}=0|_{\mathrm{seabed}} \tag{4}$$

$$A_v\frac{\partial u}{\partial z}=Su|_{\mathrm{seabed}} \tag{5}$$

$$\frac{\partial u}{\partial z}=0|_{\mathrm{surface}} \tag{6}$$

$$w=\frac{\partial \zeta}{\partial t}+u\frac{\partial \zeta}{\partial x}|_{\mathrm{surface}}. \tag{7}$$

[24] The flow and the sea bed are coupled through the continuity of sediment (equation (8)). Note that here h depends on time, in contrast with the equations for the flow. We assume the total bed sediment flux is reasonable described by the bed load formulation after *Komarova and Hulscher* [2000, equation (9)]

$$\frac{\partial h}{\partial t}=-\frac{\partial q_b}{\partial x} \tag{8}$$

$$q_b=\alpha|\tau_b|^b\left[\tau_b-\lambda|\tau_b|\frac{\partial h}{\partial x}\right]. \tag{9}$$

Grain size and porosity are included in the proportionality constant α, with the assumption that the grain size is uniform. τ_b is the shear stress at the bottom, h is the bottom elevation with respect to the mean water depth H and the constant λ takes into account that sand is transported more easily downhill than uphill. λ is related to the angle of repose and is typically 1.7 (Table 3). For more details, we refer to *Komarova and Hulscher* [2000] and *Van den Berg and Van Damme* [2006]. Using the assumption of weak nonlinearity, the fastest growing mode found in the initial stage stays the preferred wave length in the nonlinear stage. The growth toward the final shape can then be studied using

Table 3. Parameter Setting for the Sand Wave Code Simulations[a]

Parameter	Value	Unit
A_v	0.03	m^2/s
S	0.05	m/s
D	800	μm
λ	1.7	dimensionless
α	0.3	dimensionless
H_{wd}	15–60	m
Transect 1 (deep)	60	m
Transect 1 (shallow)	40	m
Transect 2 (deep)	60	m
Transect 2 (shallow)	35	m
Transect 3 (shallow)	15	m
Transect 4 (deep)	40	m
Transect 4 (shallow)	30	m
U_{osc}	0.4–1.4	m/s
Transect 1 (deep)	1.4	m/s
Transect 1 (shallow)	1.4	m/s
Transect 2 (deep)	1.0	m/s
Transect 2 (shallow)	1.0	m/s
Transect 3 (shallow)	0.45	m/s
Transect 4(deep)	1.0	m/s
Transect 4(shallow)	1.0	m/s
U_{uni}	0.3–0.7	m/s
Transect 1 (deep)	0.7	m/s
Transect 1 (shallow)	0.3	m/s
Transect 2 (deep)	0.5	m/s
Transect 2 (shallow)	0.3	m/s
Transect 3 (shallow)	0.3	m/s
Transect 4 (deep)	0.3	m/s
Transect 4 (shallow)	0.3	m/s

[a]Where only one value is given, it holds for all transects.

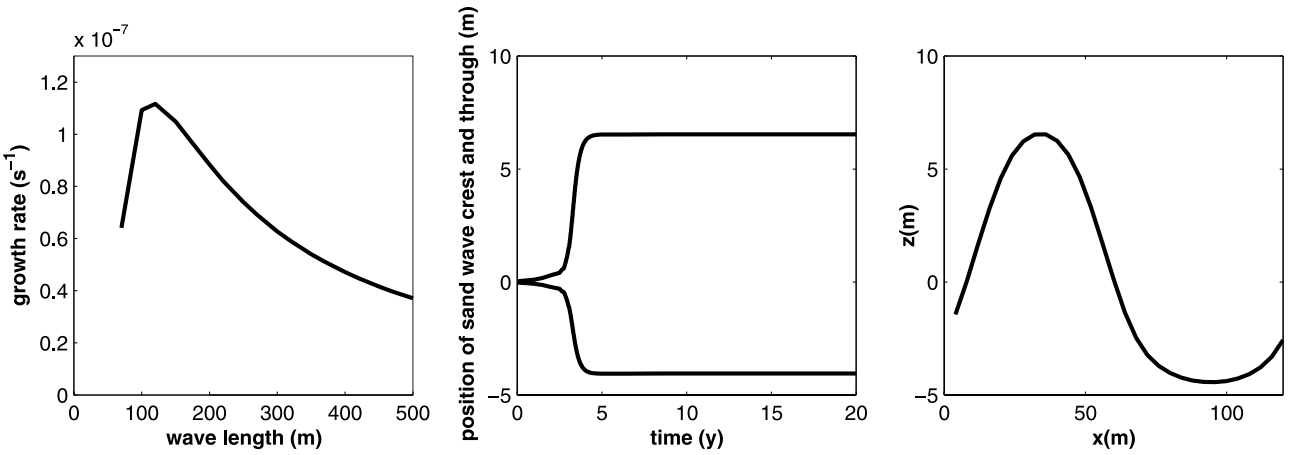

Figure 7. (left) Prediction of the fastest growing mode, growth in height is largest for a wave length of 120 m. (middle) Growth of the crest and trough of the FGM in time. (right) Predicted final sand wave form.

a fixed domain equal to one or more of these lengths. Therefore, we use a fixed domain with periodic boundary conditions in the horizontal direction. This forces all values at the inflow and the outflow boundaries to be equal. A physical interpretation is that the modeled sand wave and the tidal flows are periodic on the scale of the domain.

[25] In the actual numerical simulations, the domain of a perturbed bed is mathematically transformed to a domain with a flat bed and a flat water surface, such that a rectangular structured grid can be used. The SWC uses an staggered grid, rectangular in the 2DV plane. The grid is uniform in the horizontal and nonuniform in the vertical to obtain more resolution near the seabed.

[26] Default input parameters are listed in Table 3. Some typical model results are shown in Figure 7, using parameters as listed in Table 3, corresponding to the shallow part of transect 2. The final sand wave shape is found in two steps. First, the growth in height corresponding to various wave lengths is simulated leading to the wave length that induces the fastest growth in height (fastest growing mode (FGM), Figure 7 (left)). In this example, this is a wave length of 120 m. Secondly, for the FGM a long-term simulation finds the final shape for this sand wave, i.e., the sand wave shape that is in equilibrium with the flow and does not change over time anymore (Figure 7 (middle and right)). In this case it takes approximately 8 years to reach the final state, which has a sand wave height around 10 m. In this example, only an oscillating current is taken into account, resulting in a symmetric sand wave (Figure 7 (right)) that does not migrate. Using these two steps, the SWC is able to predict wave length, height, asymmetry, growth rate and migration. Following this approach sand wave variation can also be studied using random small initial disturbances in the bed with a larger domain (see section 4.4).

4. Results

[27] The SWC is applied to the transects described in section 2 using the parameters in Table 3. In this A_v is taken equal to previous studies in the North Sea [*Van den Berg and Van Damme*, 2006; *Németh et al.*, 2006] and the slip parameter S is taken slightly higher than previously to account for the larger grain size (see *Besio et al.* [2004], *Hulscher* [1996], and *Németh et al.* [2007] for more details about A_v and S). The value of λ is taken as 1.7, corresponding to an angle of repose of 30° for the sediment. At various locations on each transect, the water depth and flow velocity varies. The local flow is estimated using results of 2DH Delft3D simulations and from the measurements of *Cheng and Gartner* [1984]. Transect 1 and 2 are each divided into a deep part and a shallow part, to account for the large difference in water depth and the corresponding differences in measured sand waves. For transect 3 only one water depth is used in the simulations because neither the water depth nor the sand waves show large differences over the transect. Transect 4 is divided into a deep part and a shallow part, but the measured sand wave shape is derived from applying the BTT over the entire transect because the measured variation is small.

[28] First, the influence of the oscillating and unidirectional flow components are investigated to find out how well this simplified flow description is able to predict the sand wave shape. Next, the robustness of the model results is tested with a sensitivity analysis for A_v, S, and λ. Finally, simulations on a longer domain and with random initial bed disturbances investigate the possible variation due to initial conditions within a sand wave transect.

4.1. Symmetric Forcing

[29] The first simulations contain only an oscillating flow and bed load sediment transport. Results are compared with data in Table 4 and Figures 9–12 (with field measurements in Figures 9–12 (top), model results with a symmetric forcing in Figures 9–12 (middle)). Note that at this stage the simulations are carried out with a horizontal domain equivalent to the sand wave length. For convenience, i.e., easier comparison with the data, we show multiple sand waves in the Figures 9–12 by simply repeating the same bed form. Note that the location of the crests in the model results compared to the sand wave crests in the field data are arbitrary.

[30] With symmetric forcing (Figures 9–12 (middle)), the simulated sand waves are symmetric around the crest and do

Table 4. Results From Field Measurements Combined With Results From the Sand Wave Code[a]

		H_{sw}			L_{sw}		
Profile	H_{wd}	Minimum	Mean	Maximum	Minimum	Mean	Maximum
1 BTT	40	1.8	2.5	3.2	50	53	60
1 Sym	40		13			150	
1 Asym	40		3.9			70	
1 BTT	60	3.5	4.9	7.1	80	92	110
1 Sym	60		4–11			270	
1 Asym	60		3.0			100	
2 BTT	35	0.9	2.1	4.3	60	158	260
2 Sym	35		11			120	
2 Asym	35		3.7			70	
2 BTT	60	2.6	4.1	5.3	80	95	120
2 Sym	60		20			250	
2 Asym	60		3.5			100	
3 BTT	14	0.5	0.6	0.8	15	21	25
3 Sym	15		9			70	
3 Asym	15		2.8			50	
4 BTT	33	1.7	*	*	70	*	*
4 Sym	30		9			100	
4 Asym	30		2.9			50	
4 BTT	37	2.2	2.5	2.7	85	100	115
4 Sym	40		14			150	
4 Asym	40		3.7			70	

[a]Sym denotes results of the symmetrical case, and Asym denotes the results of the asymmetric case. Asterisks indicate that for this transect BTT could only use the characteristics of 1 sand wave. Model input parameters are shown in Table 3.

not migrate, in contrast to the measured waves. However, even with symmetric forcing asymmetry in sand wave shape does occur around the horizontal axis, resulting in differences between the trough and the crest. All results show longer troughs and shorter crests.

[31] We observe that the sand wave shape is not simulated realistically in these simulations, i.e., with only sinusoidal tides. Predicted sand wave heights are larger than observed, with predicted heights as large as 60% of the water depth on the shallow transect 3. Most of the predicted sand wave heights are about 30%, which is greater than found in nature. When focussing on the wave length a less negative view arises. With one exception (i.e., the shallow part of transect 2, where the simulated wave length is consistent with the observed wave length), simulated lengths are larger than observed lengths but typically within a factor 2 to 3.

4.2. Asymmetric Forcing

[32] The tidal ellipses resulting from the 2DH Delft3D modeling are not symmetrical but shifted (Figure 8). To account for this as simple as possible in the simulations, a constant flow component is implemented in addition to the oscillating flow component. To estimate the constant flow component, maximal flow in both directions were estimated from the Delft3D modeling. From this the U_{osc} was determined as the smallest value of these two and U_{uni} is determined as the difference between the two values. For example, the maximum flow velocities for the shallow part of transect 1 are 1.6 m/s seaward (Figure 8), leading to forcing the SWC with an oscillating flow component of 1.3 m/s and an unidirectional flow component of 0.3 m/s. Table 3 shows the values for all transects.

[33] Table 4 and Figures 9–12 show the results of the simulations including the additional unidirectional flow component (Figures 9–12 (bottom)). Both the shape and height of the simulated sand waves approximate the measurements significantly better than the previously described simulations using only symmetric tidal forcing. In all cases the sand wave lengths are closer to the observed wave lengths, and the simulated sand wave shape asymmetry is similar to the observed asymmetry. Also striking is that the simulated sand wave heights are much closer to the measured values as listed in Table 4. The only exception is for transect 3, where the simulated sand wave height is still five times the observed height, and the sand wave length is about twice as long as observed. Taking into account the simplifications in the model and its accuracy, the overall results describe the height and length of the observed sand waves remarkably well. Both over- and underestimations occur, but these are always less than 1 m for sand wave height (excluding transect 3). For the sand wave length only three estimations are outside the measured range; transect 1 (deep) is 10 m longer, transect 3 is 25 m longer and transect 4 (shallow) is 10 m shorter (compared with the measured data from the whole transect). These differences between the measured and the simulated wave lengths are all within the precision of the model simulations. The results are summarized in Figure 13.

[34] The residual currents also cause the sand waves to migrate in the simulations. Because of the relatively large residual current, which is perpendicular to the sand wave

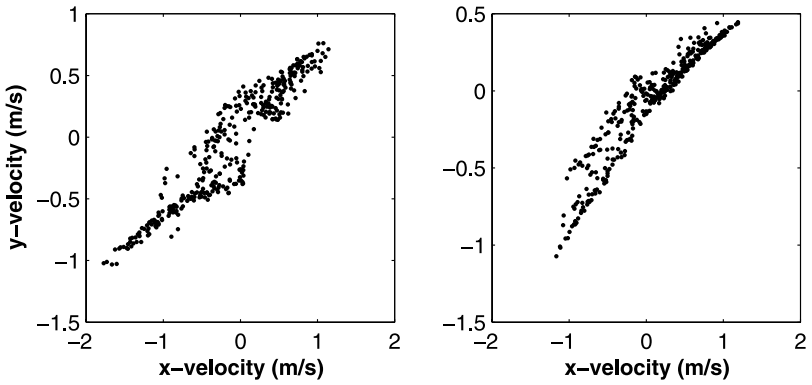

Figure 8. Tidal ellipses from transect 1, for 1 month, from 2DH simulations in Delft3D. Flow velocity components for the (left) deep and (right) shallow end of transect 1 in Figure 1.

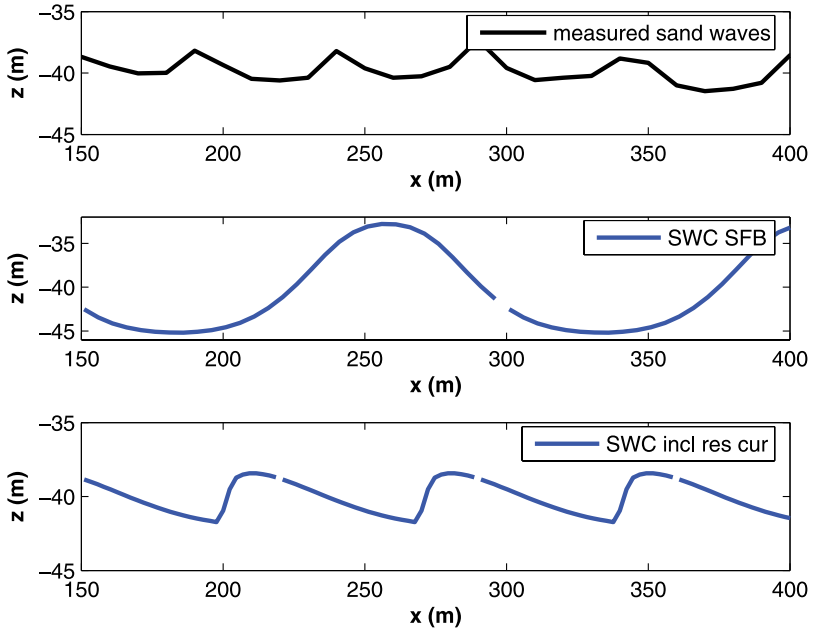

Figure 9. Measured and modeled sand wave shapes for the shallow part of transect 1. (top) The measured bed level, (middle) the final state of the basic simulation using oscillatory forcing only, and (bottom) the final state of the simulations including U_{uni}.

crest, growth and migration are both more rapid. The sand waves grow toward their final shape in approximately 1–2 years. They migrate in the direction of the residual current, at rates more than 150 m/a. Where the simplified description of the flow consisting of an oscillating and a unidirectional component adequately predicts the sand wave morphology, the sand wave dynamics appear to be overpredicted.

[35] One could argue that implementing a residual current has the same result as increasing the oscillating flow component on the sand wave morphology. In that case the results perhaps do not improve because of the unidirectional component but rather because of a higher flow velocity. Table 5 shows the results of simulations where the flow was increased by either increasing the symmetric component or by increasing the asymmetric component. It shows that asymmetric forcing, i.e., oscillating and a residual current together, considerably decrease both the FGM and the final wave height. For smaller values of the residual current, this effect is even stronger. A small residual current decreases the sand wave height (−50%) and the sand wave length (−33%). Larger residual currents increase these trends though the relative effect becomes smaller. On the contrary,

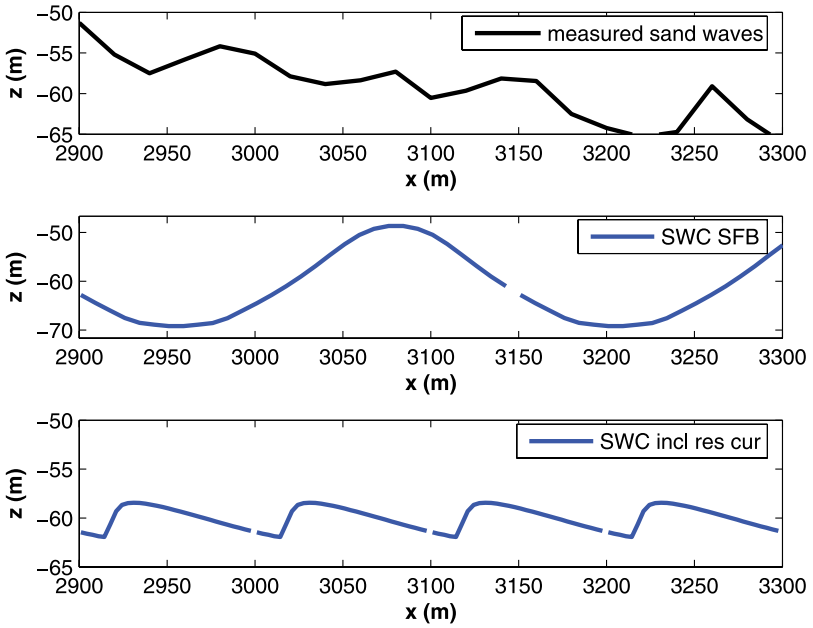

Figure 10. As in Figure 9 except for the deep part of transect 2.

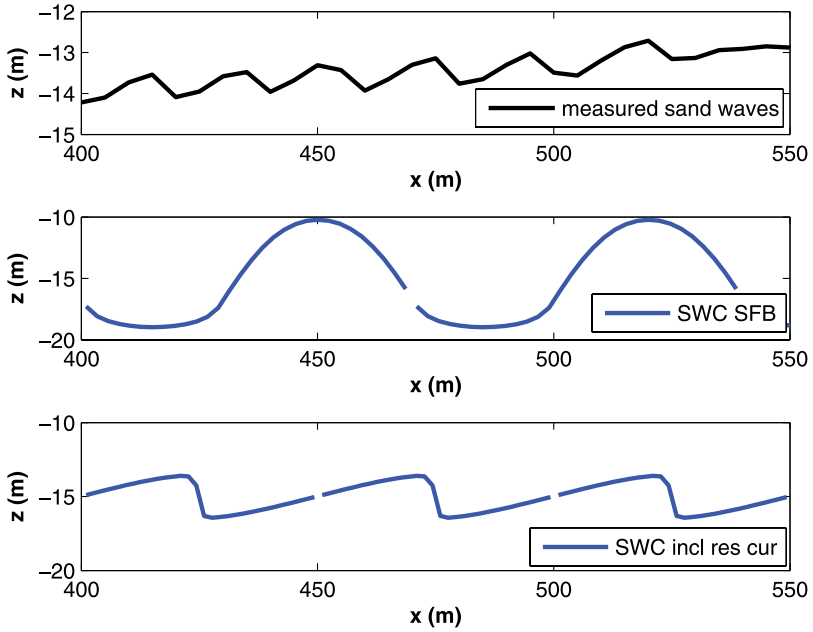

Figure 11. As in Figure 9 except for transect 3.

increasing the oscillating current with no unidirectional current only increases both the sand wave length and the sand wave height, though the changes are small compared to the model accuracy. Hence, besides reproducing the sand wave shape better, we found that a residual current also has considerable influences on the sand wave length and height.

4.3. Sensitivity Analysis

[36] We tested the sensitivity of the model results for three model parameters, the viscosity A_v, the slip parameter S and the slope term λ. These are the most difficult model values to estimate in a physically realistic way [*Németh et al.*, 2007]. Figure 14 shows the variation in final sand wave height and length resulting from changes of all three parameters. The value of the eddy viscosity A_v and the slip parameter S are varied with approximately 60% of their default value (respectively 0.1, 0.3 and 0.5 m^2/s and 0.2, 0.5, and 0.8 m/s). This is in the range of realistic values [*Hulscher and Van den Brink*, 2001; *Besio et al.*, 2004]. The slope factor λ was taken 1.2, 1.7 and 2.2, corresponding with angles of repose of 40, 30 and 24°.

[37] Figure 14 shows that the influence of A_v varies between the different transect locations. In general, increasing A_v increases the sand wave height. The influence of A_v on the sand wave length is less pronounced, and shows a tendency to stay constant. This is in agreement with the linear sensitivity analysis carried out by *Németh et al.*

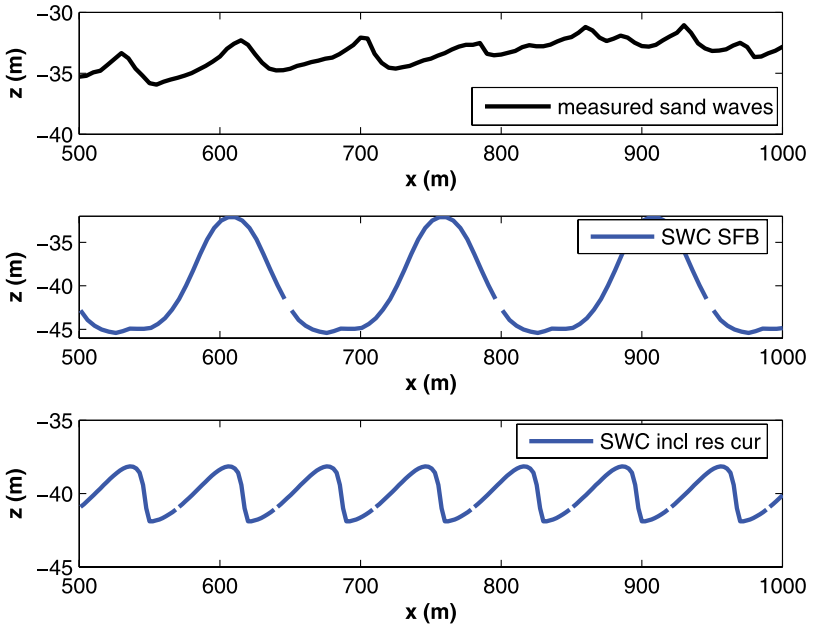

Figure 12. As in Figure 9 except for the deep part of transect 4.

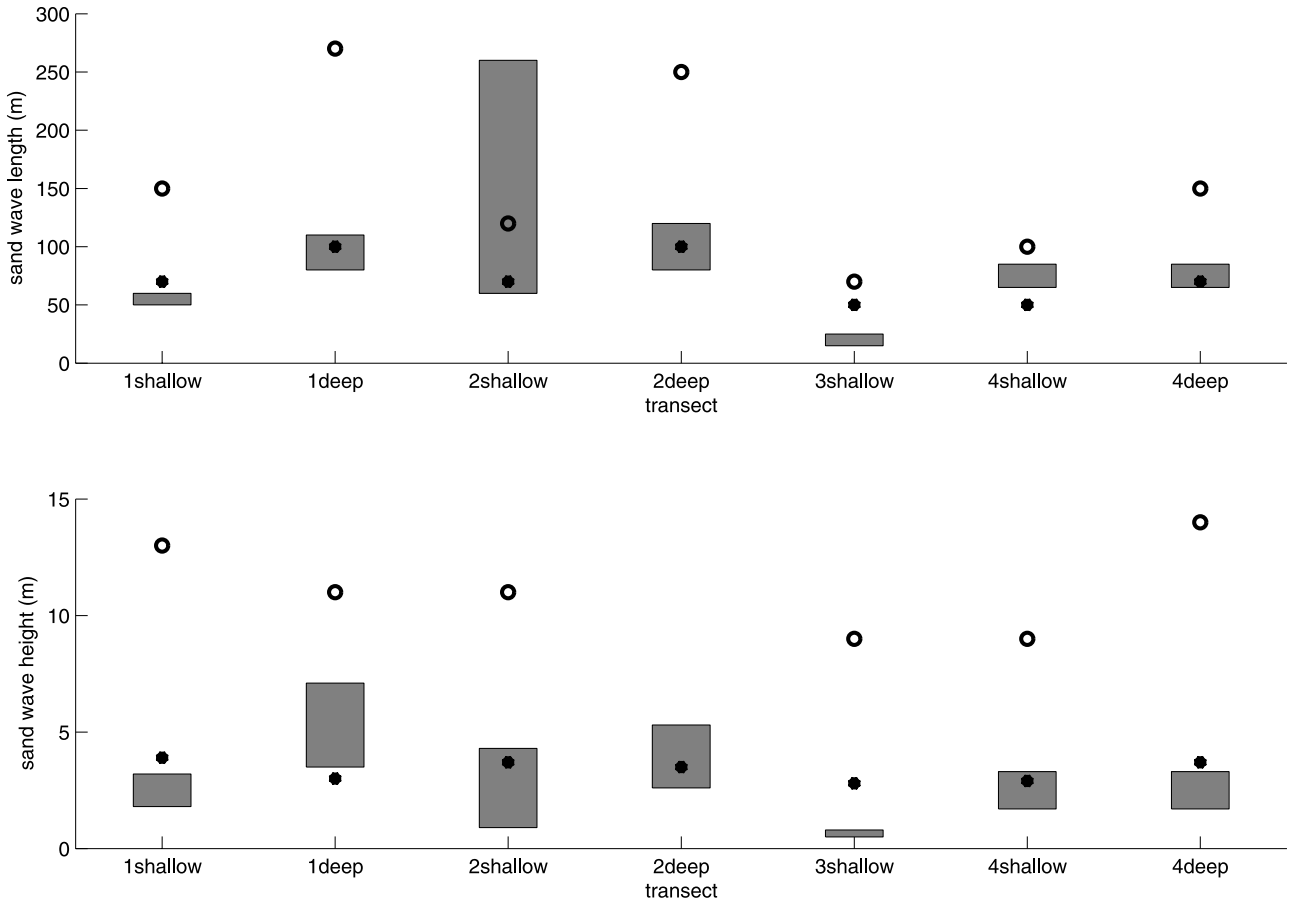

Figure 13. Comparison of the symmetric and asymmetric model results with the field data. The open circles represent the symmetric results, and the solid circles represent the asymmetric results. The grey bars indicate the range of values found in the field data.

[2002]. As the bed shear stress is the dominant factor in the initial sand wave growth, the A_v (which mostly influences the effect of changes in the flow on the vertical flow distribution) is of minor importance on the sand wave length. An exception is the deep part of transect 1, here an increase of A_v decreases both wave length and wave height. This is most likely due to the combination of the large water depth and the high flow velocity. Both values are on the edge of values where sand waves are expected [*Wilkens*, 1997]. Changing the combination of A_v and S will in this case probably sometimes result in circumstances under which sand waves are not likely to occur. The large changes in both sand wave length and sand wave height are an indication of this. The increase of A_v also increases the sand wave height because of a changing ratio of sand wave height to sand wave length (H/L). This change in H/L is the result of two processes. Firstly, the shear stress, averaged over a tidal cycle, directs sediment toward the crest. Secondly the slope of the sand wave leads to sediment transport downhill. As the shear stress equals $A_v \frac{\delta u}{\delta z}$ at the bed, an increase of A_v will lead to an increase of shear stress, changing the ratio of H/L. This results in an increase of the sand wave height as the sand wave length stays constant.

[38] Increasing the slip parameter, S, results in a decrease of bed shear stress. Both the sand wave length and the sand wave height decrease with an increasing slip parameter (decreasing stress). The decrease in sand wave length can be understood, as increasing stress dampens the smaller wave length more effectively. Decreasing this stress allows these smaller wave lengths to grow, which agrees again with *Németh et al.* [2002]. The decrease in sand wave height is the result of a combination of two processes. Firstly, because of the shorter sand wave lengths, sand waves grow to lower heights because of the constant λ. On the other hand an increase of roughness results in higher sand waves. This combination results in lower sand waves, while the ratio of height to length increases.

Table 5. Results From Several Simulations in Which the Forcing due to an Oscillatory and Steady Current is Varied Such That the Total Maximum is the Same[a]

U_{tot} (m/s)	U_{osc} (m/s)	U_{uni} (m/s)	L_{sw} (m)	H_{sw} (m)
1.5	1.5	0.0	150	12.1
1.5	1.4	0.1	100	6.6
1.7	1.7	0.0	170	13.2
1.7	1.4	0.3	70	3.8
1.9	1.9	0.0	170	12.9
1.9	1.4	0.5	70	3.3

[a]The simulations were carried out for the shallow part of transect 1.

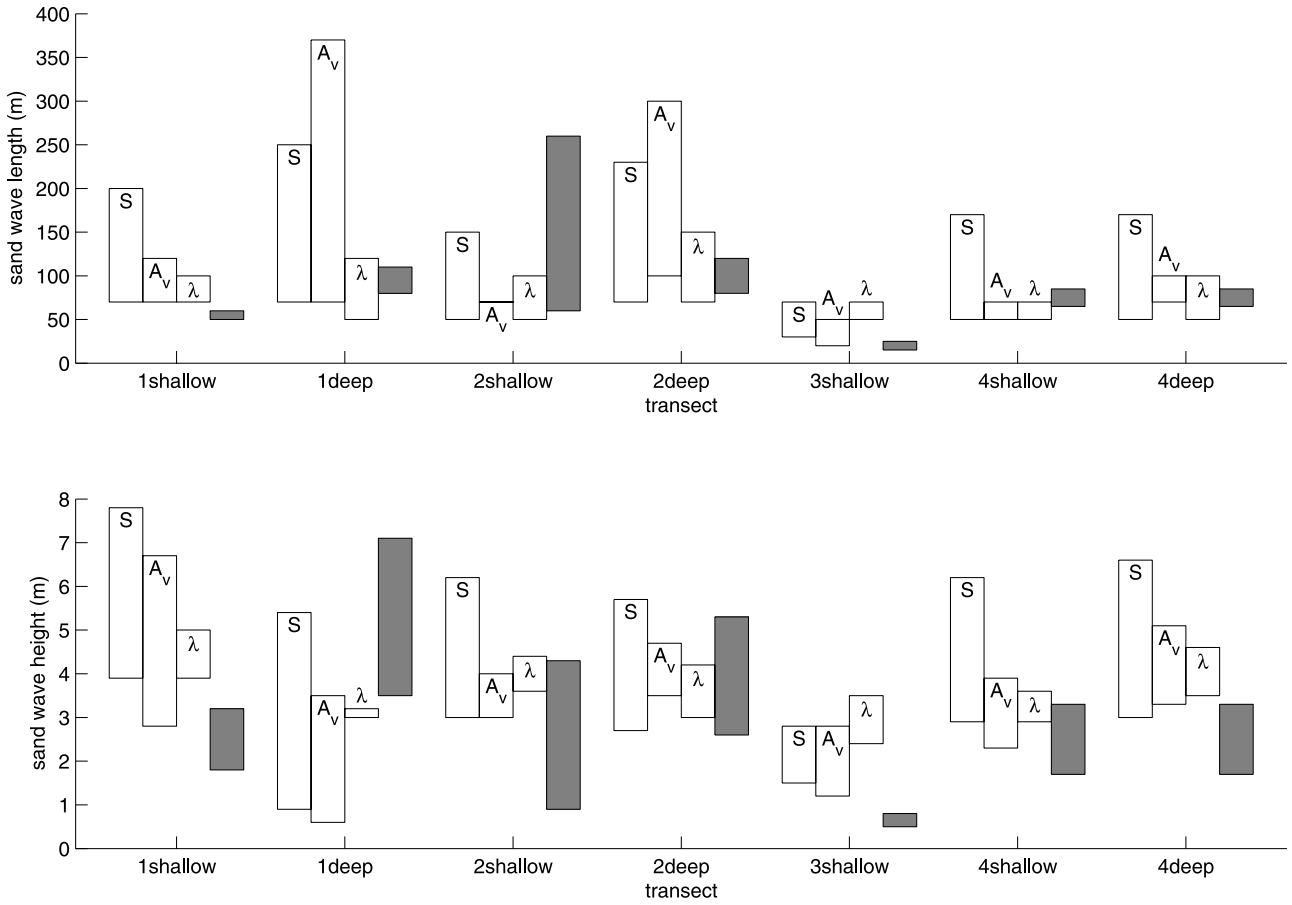

Figure 14. The influence of varying A_v, S, and λ on the model results compared with the field data (grey bar). (top) The effect on the sand wave length, and (bottom) the effect on the sand wave height.

[39] Changing λ is of minor importance to the model results according to Figure 14. Increasing λ means that the angle of repose will decrease such that the ratio between sand wave height and length decreases. As increasing λ dampens shorter waves, increasing λ results in slightly longer sand waves. The sand wave height is determined mostly by the value of the height to length ratio, and balances the change of the wave length. This leads to an increase in the wave length, except for transect 3. The wave height also increases, with only a few exceptions.

[40] The sensitivity to both A_v and S is largest on the deep part of transect 1, for reasons explained earlier. For the other transects variation is clearly visible. The value of λ seems to be of minor importance. Changing any of these model parameters does not produce drastic changes in the results. The order of magnitude of both sand wave length and sand wave height stays the same.

4.4. Random Initial Bed Perturbation

[41] All previous runs started with a domain of one sand wave length, corresponding to the FGM, with a sinusoidal initial small bed perturbation. This allows us to study the evolution of a single sand wave, while fixing its wave length. It gives insight in the variation between locations, caused by variation in the processes such as flow velocity and water depth. However, this approach cannot study the possible wave length evolution and the interaction between adjacent sand waves. To investigate these two aspects, Figure 15 shows three runs on a larger domain starting from random initial bed perturbations, with a maximal amplitude of 0.1 mm. Parameters correspond to the shallow part of transect 1.

[42] Figure 15 shows considerable sand wave variation within a location. The initial conditions lead to a variety of sand wave shapes. However, the overall statistical characteristics of each run are comparable. The sand waves tend to grow both higher and longer, though in wave length this mainly means lengthening of the troughs while the crest length stays roughly the same for the three runs.

[43] A disadvantage of this long domain simulation is that the sand wave eventually evolve to one large bed form, with a length equal to the model domain. This is caused by the fact that larger waves are not damped but in contrast show a small positive growth rate. In the long-term domain length waves overtake the smaller sand waves. At this moment the only way to overcome this weakness is to reduce the model domain to the length of the FGM. This topic is left for future research. Note that, Figure 15 shows the results after several years, and the bed is still evolving.

5. Discussion

[44] The addition of an unidirectional current exerts a strong influence on the simulated dimensions and shape of

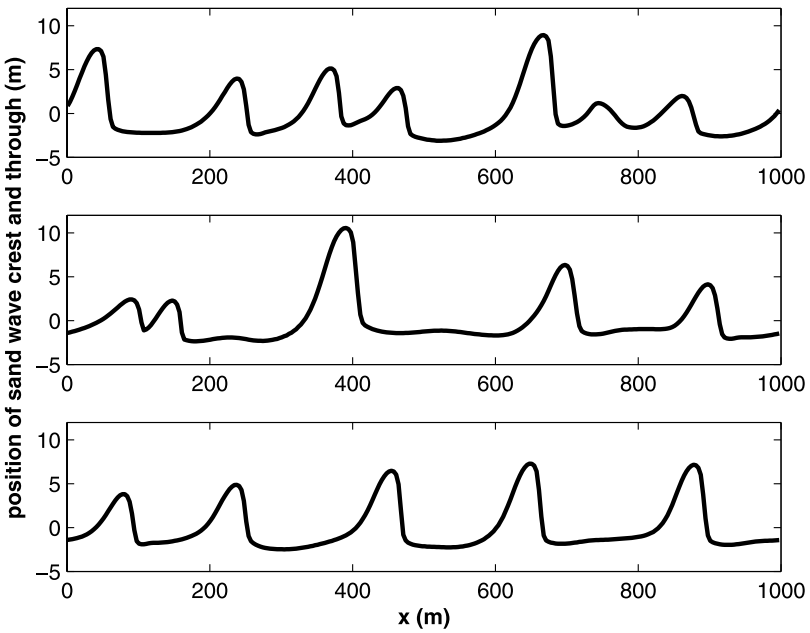

Figure 15. Simulations on a larger domain, with random initial disturbances of the order of 10^{-4} m. These profiles are still evolving with time.

the sand waves. In the idealized SWC, the simple combination of an oscillating and a residual current predicts the sand wave morphology well. If the goal is to predict the basic dimensions of the sand waves, it seems sufficient to model the flow using these two components, and not include the precise tidal constituents. This coincides with *Németh et al.* [2002], where the M_0 and M_2 are assumed to give the largest contributions to the tidal system. Further investigations which incorporate higher harmonics should test this expectation, including the effects on sand wave dynamics.

[45] Although flow separation is not included in the SWC, it is possible that flow separation occurs on these sand waves in some locations and at some times. Because of the relatively strong unidirectional current, the simulated lee slopes in transect 3 and the shallow part of transect 1 became steeper (around 30 and 15°, respectively) than the 14° that is typically needed for flow separation [*Paarlberg et al.*, 2006]. The other locations show slopes around 8–12°. *Paarlberg et al.* [2007] show that flow separation in the case of river dunes can be parameterized and modeled such that the separation streamline is captured well. As river dunes occur in purely unidirectional flow, flow separation is a critical issue when describing the flow-bed interaction. As Paarlberg uses the same basic model as used in this paper [*Van den Berg and Van Damme*, 2006], their parameterization could be included if observations would show the occurrence of flow separation over the steeper Golden Gate sand waves. Still, the present results predict the sand wave morphology well, and support the underlying hypothesis of residual circulation cells as the main process for sand wave occurrence. If flow separation does occur on these sand waves, the effects maybe limited to influencing the detailed shape of the sand waves, particularly near the crests, as well as the sediment transport due to smaller superimposed bed forms in this region.

[46] When comparing the model results with the data, one should remember the model is idealized and accuracy for the modeled sand wave height are around 15%, due to possible instabilities in the final shape. Accuracy for the sand wave length is around 20–30 m. Also section 4.4 shows that variation in the field occurs frequently, while in the model, using one wave only, this variation is not taken into account. Though results in section 4.4 are not realistic in the sense that sand waves grow too large, they give a good indication of the possible variation over the area due to random initial conditions. More variation is likely to occur because of the ever present natural random fluctuations. This variation cannot yet be properly included in the model without greatly increasing the computation time. In light of the above considerations, the model results compare reasonably well with the data. When transect 3 is excluded both the predicted sand wave length and the predicted sand wave height are in range with the observed values (Figure 13). Small over and small under estimations exists, but these are all in range of the model accuracy.

[47] Though the SWC results are influenced by varying the value of A_ν, S, and λ this influence is of minor importance compared to the range in predictions possible over the whole area, i.e., the variation that exists between the transects. Even though the variation in circumstances over the region are large, predictions with the default values were reasonable over the whole area. It is worth mentioning that the model parameters were not tuned to fit the data. General values are used for A_ν, S, and λ. The sensitivity analysis further shows that the model results are robust for a range of these values.

[48] For transect 3, the model results compare significantly less well to the observations than for the other transects. We used a grain size of 800 μm, corresponding to typical measurement on the seabed surface on transect 0. However, grain size varies substantially in the region. Especially in transect 3 we can expect smaller grain sizes

as measurements closer to the coast show smaller grains. This would lead to a smaller value of S, which would lead to larger sand waves (Figure 14) and would not solve the difficulties the model has on this transect. The residual current estimation might be another cause of error. Transect 3 is located in a region with particularly complex waves and currents. A reversing counterflow eddy is frequently present in the vicinity of transect 3. In addition, the steep bathymetric slopes and strong jet-like currents in the region cause complex surface wave patterns, with sharp gradients in wave characteristics. Runs for transect 3, with different residual currents, showed that increasing the residual current reduces both the sand wave length and height (e.g., for a residual current of 0.5 m/s sand wave height and length are 30 and 1.6 m, respectively). However, this increase in flow conditions to fit the observed data is beyond the expected values of both the residual current and the maximal flow velocity. Another possible reason for the misprediction on transect 3 is that because of the shallower water, wind and short waves have more impact on the seabed, changing the bed forms. Research on the influence of surface gravity waves shows that they can lower the sand wave heights significantly (F. M. Sterlini et al., Modelling the effect of surface waves on offshore sand waves, manuscript in preparation, 2009).

[49] The sand waves in the mouth of San Francisco Bay are located on the edge of a large ebb tidal delta. The unusual bed slope might affect the migration of sand waves as well as their shape. While the sand wave shape indicates potential migration in the seaward direction, the slope due to the ebb tidal delta may counteract this potential migration.

[50] The model results in this paper include bed load sediment transport only. In most cases this is a good assumption, however, on transects 1 and 2 it is likely that suspended sediment transport takes place, because of the high velocities during peak tide (w_s/u_* is smaller than 1). Note that these high velocities only occur during a part of the tidal cycle (Figure 4). Further research is under way concerning the influence of suspended sediment transport on the sand wave morphology and dynamics. First results indicate that the inclusion of suspended sediment slightly lowers and shortens the sand waves. In addition their shape changes toward more trough-crest asymmetry; the trough becomes longer and the crest shorter. This coincides with field observations. The overall results of the present model without suspended sediment are not changed qualitatively.

6. Conclusions

[51] In this paper we present a detailed comparison between sand wave measurements and nonlinear sand wave model simulations. The main question addressed is: "Can a simplified nonlinear model explain sand wave variation between locations with different forcing conditions?"

[52] The results of the simulations show that the model is able to describe the variation in the Golden Gate sand waves well. The results of the SWC compare reasonably well with the observed sand waves when both an oscillating and a residual current are taken into account. Except for transect 3, it is sufficient to implement this forcing and bed load sediment transport to predict the sand wave height, length and shape close to the observed values for the different locations. Current together with water depth seem to be the most important factors influencing sand wave characteristics. To model wave length, height and shape correctly it is crucial to include the local residual current. Though the value of both the constant eddy viscosity and the slip parameter influence the wave length and height, adjusting from the default values does not significantly improve the comparison with the field measurements.

[53] Large-domain simulations give an indication of expected variation within a single transect. However, in these large domain simulations no realistic final state could be established.

[54] The validation of the simulations gives further confidence in the underlying hypothesis and assumptions. The feedback mechanism between the bed forms and the tidal flow seems to be the leading process. The assumption that the sand waves are weakly nonlinear, i.e., we can use the preferred wave length from the linear regime, is supported by the good comparison of the model results with the highly variable field data.

[55] **Acknowledgments.** F.S. is supported by the Technology Foundation STW, Applied Science Division of NWO, and the Technology Programme of the Ministry of Economic Affairs; their support is gratefully acknowledged. The authors would like to thank Edwin Elias for the stimulating discussions and critical reviews of this work, Jingping Xu for his useful review, Rolien van der Mark for the use of the BTT, Joris van den Berg for the use of the SWC and good cooperation, and the associate editor for his helpful comments.

References

Barnard, P. L., D. M. Hanes, D. M. Rubin, and R. G. Kvitek (2006), Giant sand waves at the mouth of San Francisco Bay, *Eos Trans. AGU*, *87*(29), 285–286, doi:10.1029/2006EO290003.

Barnard, P. L., J. L. Eshleman, L. Erikson, and D. M. Hanes (2007), Coastal processes study at Ocean Beach, San Francisco, CA: Summary of data collection 2004–2006, *Open-File Rep. 2007-1217*, 165 pp., U. S. Geol. Surv., Reston, Va. (Available at http://pubs.usgs.gov/of/2007//1217/.)

Besio, G., P. Blondeaux, M. Brocchini, and G. Vittori (2003a), Migrating sand waves, *Ocean Dyn.*, *53*, 232–238.

Besio, G., P. Blondeaux, and P. Frisina (2003b), A note on tidally generated sand waves, *J. Fluid Dyn.*, *485*, 171–190.

Besio, G., P. Blondeaux, M. Brocchini, and G. Vittori (2004), On the modeling of sand wave migration, *J. Geophys. Res.*, *109*, C04018, doi:10.1029/2002JC001622.

Cheng, R. T., and J. W. Gartner (1984), Tides, tidal and residual currents in San Francisco Bay, California: Results and measurements, 1979–1980, *Water Resourc. Invest. Rep. 84–4339*, U. S. Geol. Surv., Reston, Va.

Dodd, N., P. Blondeaux, D. Calvete, H. de Swart, A. Falqués, S. J. M. H. Hulscher, and G. Vittori (2003), Understanding coastal morphodynamics using stability methods, *J. Coastal Res.*, *19*(4), 849–866.

Hulscher, S. J. M. H. (1996), Tidal-induced large-scale regular bed form patterns in a three-dimensional shallow water model, *J. Geophys. Res.*, *101*, 727–744.

Hulscher, S. J. M. H., and G. M. Van den Brink (2001), Comparison between predicted and observed sand waves and sand banks in the North Sea, *J. Geophys. Res.*, *106*(C5), 9327–9338.

Komarova, N. L., and S. J. M. H. Hulscher (2000), Linear instability mechanisms for sand wave formation, *J. Fluid Mech.*, *413*, 219–246.

Németh, A. A., S. J. M. H. Hulscher, and H. J. De Vriend (2002), Modelling sand wave migration in shallow shelf seas, *Cont. Shelf Res.*, *22*(18), 2795–2806.

Németh, A. A., S. J. M. H. Hulscher, and R. M. J. Van Damme (2006), Simulating offshore sand waves, *Coastal Eng.*, *53*, 265–275.

Németh, A. A., S. J. M. H. Hulscher, and R. M. J. Van Damme (2007), Modelling offshore sand wave evolution, *Cont. Shelf Res.*, *27*, 713–728.

Paarlberg, A. J., C. M. Dohmen-Janssen, S. J. M. H. Hulscher, J. Van den Berg, and P. Termes (2006), Modelling morphodynamic evolution of river dunes, in *River Flow 2006*, edited by R. M. L. Ferreira et al., pp. 969–978, Taylor and Francis, London.

Paarlberg, A. J., C. M. Dohmen-Janssen, S. J. M. H. Hulscher, and P. Termes (2007), A parameterization of flow separation over subaqueous dunes, *Water Resour. Res.*, *43*, W12417, doi:10.1029/2006WR005425.

Van den Berg, J., and D. Van Damme (2006), Sand wave simulations on large domains, in *River, Coastal and Estuarine Morphodynamics: RCEM 2005, Urbana, Illinois, USA, 4–7 October 2005*, edited by Parker and Garcia, pp. 991–997, Taylor and Francis, London.

Van der Mark, C. F., A. Blom, and S. J. M. H. Hulscher (2007), Variability in bedform characteristics using flume and river data, in *River, Coastal and Estuarine Morphodynamics: RCEM 2007*, edited by C. M. Dohmen-Janssen and H. S. J. M. Hulscher, pp. 923–930, Taylor and Francis, London.

Van der Veen, H. H., S. J. M. H. Hulscher, and M. A. F. Knaapen (2006), Grain size dependency in the occurence of sand waves, *Ocean Dyn.*, *56*(3–4), 228–234.

Wilkens, J. (1997), Sand waves and possible related characteristics, technical report, Alkyon Hydraul. Consult. and Res., Emmeloord, Netherlands.

D. M. Hanes, Coastal and Marine Geology Program, U.S. Geological Survey, 400 Natural Bridges Drive, Santa Cruz, CA 95060, USA.

S. J. M. H. Hulscher and F. Sterlini, Water Engineering and Management, Faculty of Engineering Technology, University of Twente, P.O. Box 217, NL-7500 AE Enschede, Netherlands. (f.m.vanderMeer@utwente.nl)